WAVE-DOMAIN APPROACH FOR CANCELLING NOISE ENTERING OPEN WINDOWS

Daan Ratering[⋆]*, W. Bastiaan Kleijn*[†‡]*, Jean Gonzalez Silva*[⋆]*, and Riccardo M.G. Ferrari*[⋆]

[⋆] Delft Center for Systems and Control and [‡] Dept. Microelect., Delft Univ. of Technology, Netherlands
[†]School of Engineering and Computer Science, Victoria University of Wellington, New Zealand

ABSTRACT

Active control of noise propagating through apertures is commonly realized with closed-loop LMS algorithms. However, these algorithms require a large number of error microphones and provide only local attenuation. Slow convergence and high computational effort are additional disadvantages. We propose a wave-domain approach that converges instantaneously, operates with low computational effort and does not require error microphones. It inherently controls sound in all directions in the far-field. The soundfield from the aperture is matched in a least squares sense with the generated soundfield from the loudspeaker array using orthonormal basis functions. Compensation for algorithmic delay, induced by blockwise processing, can be based on microphone placement or signal prediction, at the cost of a loss in attenuation performance. Our simulation results indicate that wave-domain processing has the potential to outperform LMS-based methods in practical active noise control for apertures.

Index Terms— open window, aperture, active noise control, wave-domain algorithm, multiple-error least mean squares algorithm, algorithmic delay compensation

1. INTRODUCTION

Noise pollution is a major health threat to society [1]. Active Noise Control (ANC) systems attenuating noise propagating through open windows (apertures) have the potential to create quieter homes while maintaining ventilation and sight through the apertures [2]. ANC systems employ loudspeakers to produce anti-noise soundfields that reduce the sound energy in noise-cancelling headphones [3] or over regions such as airplane cabins [4]. Actively controlling sound propagating through open windows is being studied [5, 6]. The objective is to reduce sound energy inside the room. Current methods employ closed-loop algorithms, leading to long convergence times [7] and computational loads too high for real-time use [8]. In addition, a large number of error microphones, which block the window, are required for global control. Finally, performance decreases if sounds from inside the room reach error microphones. These drawbacks limit the feasibility of such systems [9].

Most ANC systems for apertures utilize closed-loop Least Mean Squares (LMS) algorithms, such as the well-known Filtered-x LMS (FxLMS) algorithm [7], or its multi-channel equivalent, the multiple-error LMS [7, 10]. These closed-loop algorithms aim to minimize error signals at error microphones placed in the room by adapting signals generated by loudspeakers in the aperture. Current studies indicate that LMS based ANC for apertures can obtain a 10 dB global reduction of white noise between 0.4 and 1 kHz [11] and 0.5 and 2 kHz [12]. To set a baseline, the multiple-error normalized LMS algorithm will be used as a reference system.

We thank the GN Group for funding this research.

We note that the control problem has similarities with wave-domain spatial control of the sound produced by multi-speaker sound systems, e.g. [13–16] and active cancellation of wall reflection of sound of a talking person [17], as well as wave-field synthesis [18]. Such a wave-domain algorithm uses a temporal frequency domain basis function expansion over a control region. The soundfield from the aperture and loudspeaker array can be expressed in these basis functions and their sum can be minimized in least squares sense [13–15].

In general, ANC systems for open windows with loudspeakers distributed over the aperture [6] outperform those with loudspeakers placed on the boundary of the aperture [5]. A compromise between both setups is a sparse array, that consists of a window with a cross-bar containing the speakers [19, 20].

We propose a wave-domain approach to ANC for apertures that addresses the shortcomings of the closed-loop LMS approach. It intrinsically ensures global control, because it cancels noise in all directions from the aperture, and does not require error microphones positioned. To our best knowledge, our work is the first to implement wave-domain control to open windows. Optimal filter-weights that minimize far-field sound energy for each frequency are calculated. We extend known Acoustic Transfer Functions (ATFs) that describe the sound propagation through apertures [19] and from loudspeakers [21]. The wave-domain algorithm operates in the temporal frequency domain. Hence it is necessary to transform signals with the Short-time Fourier Transform (STFT). This operation induces an algorithmic delay equal to the window-size of the STFT which can be compensated by signal prediction or microphone placement. With prediction, optimal window-size results from a trade-off between prediction performance and the algorithm performance [15].

Our contribution is the development of a wave-domain ANC for apertures that has the potential to outperform current LMS systems, and its implementation in a simulation environment. Moreover, the development of an extension to aperture ATFs [19], a procedure for basis function orthonormalization with Cholesky decomposition, and the matrix implementation of filter-weight calculation, extend current literature. An advantage of our wave-domain control system over existing LMS-based systems is that the filter weights are calculated off-line, leading to a lower computational effort. Furthermore, these coefficients are computed independent of the incoming noise. Therefore, the wave-domain approach itself requires no time to convergence. Its performance is affected by the algorithmic delay compensation method, the accuracy with which the aperture is represented and the physical characteristics of the microphone and loudspeaker arrays. In this study, both sparse and grid arrays will be used, and their performance is compared.

Section 2 formulates the problem and covers necessary ATFs. The open-loop wave-domain algorithm is developed in Section 3. Section 4 describes the reference system and evaluation methods and discusses the results. Finally, a conclusion is given in Section 5.

2. PROBLEM FORMULATION AND NOTATION

Our objective is to develop an open-loop wave-domain control algorithm that ensures global attenuation of noise propagating through an aperture. The algorithm is designed to achieve cancellation in the far-field ($r > 0.8$ m). Following Huygens' principle, the energy behind a finite control region is minimized if a wavefront, with minimized sound energy, is created in that region [22]. The aim of the algorithm is to generate such a wavefront in the control region.

Throughout the paper, $k = 2\pi f/c$ is the wavenumber, $j = \sqrt{-1}$ is the imaginary number, the unnormalized sinc function is used [21] and $[\cdot]^H$ and $||\cdot||$ are the conjugate transpose and the Euclidean norm, respectively. We use spherical coordinates with radius r, inclination θ and azimuth ϕ and corresponding Cartesian coordinates $x = r\sin\theta\cos\phi$, $y = r\sin\theta\sin\phi$ and $z = r\cos\theta$.

The noise is assumed to be a plane wave [12], with fixed incident angle (θ_0, ϕ_0). Then, we constrain the problem by modeling the aperture as a sum of square baffled pistons in an infinitely large wall with an ATF [19]. Such an ATF relates the pressure of the plane wave with the pressure of the soundfield at position $\boldsymbol{x}$ in the room. The equation, for 3D modeling, is derived from [21] as:

$$H^{ap}(\boldsymbol{x}, k, \theta_0, \phi_0) = \frac{jck\rho_0}{2\pi}\dot{\omega}_0 \Delta L_x \Delta L_y \sum_{i=1}^{\hat{P}} D_i, \tag{1}$$

where c is the speed of sound, $\dot{\omega}_0$ is a gain constant, ΔL_x and ΔL_y are aperture section dimensions and $\hat{P}$ is the number of aperture sections. D_i is the directivity, of each piston, defined as:

$$D_i = \frac{e^{-jk(r_i+\tau_i)}}{r_i}\text{sinc}\left(\frac{\Delta L_x k(\sin\theta_i\cos\phi_i - \sin\theta_0\cos\phi_0)}{2}\right) \text{sinc}\left(\frac{\Delta L_y k(\sin\theta_i\sin\phi_i - \sin\theta_0\sin\phi_0)}{2}\right), \tag{2}$$

where, for section i , r_i, θ_i and ϕ_i are the adjusted spherical coordinates and τ_i is a delay term due to the incident angle of the plane wave. Modeling in 2D is done by removing the height ΔL_x, omitting the sinc function in the x direction, and setting $x = 0$.

Furthermore, we constrain the system by modeling the ATFs of Q number of loudspeakers as monopoles [21, 23]:

$$H_q^{ls}(\boldsymbol{x}, k) = \frac{jck\rho_0}{4\pi} A_q \frac{e^{-jkr_q}}{r_q}, \tag{3}$$

in which $A_q = 4\pi a_{point}^2 u_0$ is each monopole's amplitude, with u_0 a surface velocity gain constant, a_{point} the radius of the point source and r_q the adjusted spherical radius from a monopole to a position $\boldsymbol{x}$ in the room. The soundfield from the loudspeaker array is the sum of multiple loudspeaker soundfields. The loudspeaker ATF in (3), holds in 2D and 3D.

3. WAVE-DOMAIN ALGORITHM

3.1. Basis functions and control region

We define the control region over which we want to minimize the sound pressures as a spherical shell with finite thickness in 3D: $\mathbb{D}_{3D} = \{r_{min} \le r \le r_{max}, 0 \le \theta \le \frac{\pi}{2}, 0 \le \phi \le 2\pi\}$ and an arc with finite thickness in 2D: $\mathbb{D}_{2D} = \{r_{min} \le r \le r_{max}, 0 \le \theta \le \frac{\pi}{2}, \phi = \frac{\pi}{2} \ \wedge \ \phi = -\frac{\pi}{2}\}$.

The soundfield over the control region at a single wavenumber k, denoted $S(\boldsymbol{x}, k) : \mathbb{D} \times \mathbb{R} \to \mathbb{C}$ is written as a weighted series of basis functions $\{U_g\}_{g\in\mathcal{G}}$ [14, 21]:

$$S(\boldsymbol{x}, k) = \sum_g E_g U_g(\boldsymbol{x}, k), \tag{4}$$

where $S(\boldsymbol{x}, k)$ is the soundfield, E_g are G coefficients and $U_g(\boldsymbol{x}, k)$ is a $G \times 1$ vector containing G basis functions. We assume that all feasible solutions on $\mathbb{D}$ fall in the Hilbert space spanned by the orthonormal set $\{U_g\}_{g\in\mathcal{G}}$. The inner-product is defined as $\langle Y_1, Y_2\rangle = \int_{\mathbb{D}} Y_1(\boldsymbol{x}) Y_2^H(\boldsymbol{x}) d\boldsymbol{x}$, where Y_1 and Y_2 are functions of the form $Y_1 : \mathbb{R}^3 \to \mathbb{R}$ and $Y_2 : \mathbb{R}^3 \to \mathbb{R}$. For a given $S(\mathbf{x}, k)$ and $U_g(\mathbf{x}, k)$, the coefficients E_g are obtained with $E_g = \langle S(\mathbf{x}, k), U_g(\mathbf{x}, k)\rangle$.

The orthonormal set of basis functions is obtained by starting with a set of non-orthogonal functions $f_g(\mathbf{x}, k) : \mathbb{R}^3 \times \mathbb{R} \to \mathbb{C}$ that represent G plane waves with directions evenly distributed in 3D [24]. The non-orthogonal functions are defined as plane waves: $f_g(\mathbf{x}, k) = e^{jk\mathbf{x}\cdot\hat{\beta}_g}$, where $\hat{\beta}_g \equiv (1, \theta_g', \phi_g')$ is the unit vector in the direction of the gth plane wave. We normalize each function to obtain $\hat{f}_g(\mathbf{x}, k) = \frac{f_g}{||f_g||}$ and create vector $\hat{f} = [\hat{f}_1\ \hat{f}_2 \cdots \hat{f}_G]^T$. Next, we find a lower triangular matrix R such that $U = R\hat{f}$, where U is a vector containing G orthonormal basis functions. We define:

$$F = \hat{f}\hat{f}^T = \begin{bmatrix} F_{(1,1)} & F_{(1,2)} & \dots & F_{(1,G)} \\ F_{(2,1)} & F_{(2,2)} & & \vdots \\ \vdots & & \ddots & \\ F_{(G,1)} & \dots & \dots & F_{(G,G)} \end{bmatrix}, \tag{5}$$

with inner product elements $F_{(i,j)} = \langle \hat{f}_i, \hat{f}_j\rangle$. F is symmetric and positive definite: $\mathbf{x}^H F\mathbf{x} > 0 \ \forall \ \mathbf{x} \in \mathbb{C}^n$. Then, we set $V = R^{-1}$ and obtain V by applying the Cholesky decomposition on F, where $F = VV^T$ [25]. Finally, we obtain the orthonormal set of basis functions by inverting V, where $U = V^{-1}\hat{f} = R\hat{f}$.

In literature, $G_{3D} = (ekr_{max}/2{+}1)^2$, and $G_{2D} = (\lceil 2kr\rceil{+}1)$ basis functions are suggested for the expansion over a full ball and full disc, respectively [26]. This ensures a relative truncation error, in the generated soundfield, of less than 16%, However, our 3D spherical shell control region is not a full ball. An informal parameter optimization shows that we need $G_{3D}/16$ basis functions for equivalent results, resulting computational benefits. Finally, we expect that the 16% truncation error leads to performance loss.

3.2. Weight calculation

In this subsection, we discuss the procedure to obtain filter weights $l_q(k)$ for all loudspeakers q at wavenumber k.

First, we write the soundfields of the aperture as a sum of orthonormal basis functions:

$$S^{ap}(\mathbf{x}, k) = \sum_{g=1}^{G} A_g U_g(\mathbf{x}, k), \tag{6}$$

where H^{ap} is from (1). Weights A_g are obtained with the inner product: $A_g = \langle H^{ap}(\mathbf{x}, k), U_g(\mathbf{x}, k)\rangle$, written in matrix form with coefficient vector $\boldsymbol{a} = [A_1\ A_2 \cdots A_G]^T$ and a vector containing inner products between the ATF and the normalized basis functions denoted as $\boldsymbol{H}_{\hat{f}}^{ap} = [\langle H^{ap}, \hat{f}_1\rangle \langle H^{ap}, \hat{f}_2\rangle \cdots \langle H^{ap}, \hat{f}_G\rangle]^T$. Plugging in $U = R\hat{f}$ gives: $\boldsymbol{a} = R\boldsymbol{H}_{\hat{f}}^{ap}$.

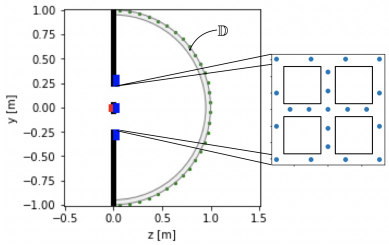

Fig. 1: 2D cross-section, with reference microphone (red), sparse loudspeaker array (blue), control region $\mathbb{D}$ and evaluation microphones (green).

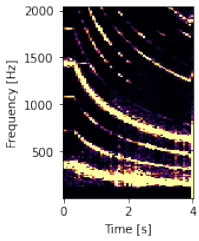

Fig. 2a: Spectrogram of rumbler signal with 32 ms window-size.

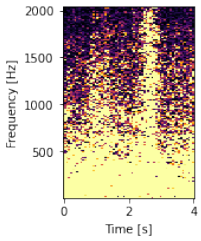

Fig. 2b: Spectrogram of airplane signal with 32 ms window-size.

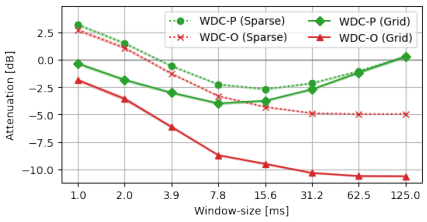

Fig. 4: 3D SNR results with optimal (WDC-O) and predictor (WDC-P) wave-domain controllers for rumbler-siren signals.

Similarly, we write the soundfield from a single loudspeaker as:

$$H_q^{ls}(\mathbf{x},k) = \sum_{g=1}^{G} C_g^q U_g(\mathbf{x},k), \tag{7}$$

with H_q^{ls} from (3) and coefficients C_g^q. The soundfield of the complete array is expanded with coefficients B_g, as well as a sum of the soundfields from all loudspeakers, multiplied by their filter weights:

$$S^{ar}(\mathbf{x},k) = \sum_{g=1}^{G} B_g U_g(\mathbf{x},k) = \sum_{q=1}^{Q} l_q(k) H_q^{ls}(\mathbf{x},k), \tag{8}$$

from which we generate coefficients B_g by (8) and (7), leading to:

$$B_g = \sum_{q=1}^{Q} l_q(k) C_g^q, \tag{9}$$

where $C_g^q = \langle H_q^{ls}(\mathbf{x},k), U_g(\mathbf{x},k)\rangle$. In matrix form we obtain:

$$\boldsymbol{C} = R\boldsymbol{H}_{\hat{f}}^{ls} = R \begin{bmatrix} \langle H_1^{ls}, \hat{f}_1\rangle & \langle H_2^{ls}, \hat{f}_1\rangle & \cdots & \langle H_Q^{ls}, \hat{f}_1\rangle \\ \langle H_1^{ls}, \hat{f}_2\rangle & \langle H_2^{ls}, \hat{f}_2\rangle & & \vdots \\ \vdots & & \ddots & \\ \langle H_1^{ls}, \hat{f}_G\rangle & \cdots & \cdots & \langle H_Q^{ls}, \hat{f}_G\rangle \end{bmatrix}. \tag{10}$$

where $\boldsymbol{H}_{\hat{f}}^{ls}$ contains the inner-products between the orthonormal basis functions ($\hat{f}_i$) and the loudspeaker ATFs (H_q^{ls}).

Finally, we set the control problem as the sum of the soundfields, $J(l_q) = S^{ap} + S^{ar}$, with $\eta = ||J(l_q)||^2$ and minimize in least mean square sense: $\min_{l_q} ||J(l_q)||^2$. With (6) and (8) gives

$$\eta = ||\sum_{g=1}^{G} A_g U_g(\mathbf{x},k) + \sum_{g=1}^{G} B_g U_g(\mathbf{x},k)||^2 = \sum_{g} |A_g + B_g|^2. \tag{11}$$

With the knowledge that $\langle U_i, U_j\rangle = 0$, we can rewrite in matrix form. We denote $\boldsymbol{b} = \boldsymbol{C}\boldsymbol{l}$, where $\boldsymbol{l} = [l_1\ l_2 \cdots l_Q]^T$. Furthermore, we add the regularization term $\tau\boldsymbol{l}$ with $\tau > 0$, to constrain the loudspeaker effort and ensure a robust solution [14]:

$$\eta = (\boldsymbol{a}+\boldsymbol{b})^H(\boldsymbol{a}+\boldsymbol{b}) + \tau||\boldsymbol{l}||^2, \tag{12}$$

where $\boldsymbol{l}$ can be found by:

$$\boldsymbol{l} = -(\boldsymbol{C}^H\boldsymbol{C} + \tau\boldsymbol{I})^{-1}\boldsymbol{C}^H\boldsymbol{a}, \tag{13}$$

in which $\boldsymbol{I}$ is an identity matrix.

3.3. Block-processing

An element-wise multiplication of the ATF with a STFT block is employed to transform signals, from the aperture and loudspeakers, to any position the room. For the STFT, the window-function, $w(n)$ of length N is chosen to fulfill $\sum_{m\in\mathcal{Z}} w(n-mH)^2 = 1$ where n is the discrete time index, m is hop-number and H is the hop-size. This ensures that we have a tight frame with perfect reconstruction [27].

The circularity property of the STFT leads to wrapping of the signals, if phase-shifts by ATFs become significant compared to the window-size. Employing zero-padding can reduce this issue, however, it emits the shifted signal content. We overcome this problem by removing the major time shift from the wave-domain multiplication and implementing it in the time-domain.

The block-processing with STFT in the wave-domain approach induces an algorithmic delay. The window-size N determines the length of the delay. Compensating for this can either be done by placing the reference microphone at a distance of at least cN/f_s in front of the aperture, or, by predicting the noise signal. We compare both methods. For prediction, an auto regressive model with *Yule-Walker estimators* predicts the incoming noise signal each STFT hop m over a prediction horizon equal to N [28].

4. RESULTS AND DISCUSSION

4.1. Reference system

The performance of the proposed open-loop wave-domain algorithm was compared with a multiple-error Normalized LMS (NLMS) algorithm [6, 10]. Its error microphones were, for fair comparison, positioned in two rows within the control region of the wave-domain controller such that soundfield minimization was done over the same region. For the algorithm, the reader is referred to [29] and [30].

4.2. Experimental setup

The 3D simulation environment represents a physical setup, entailing a window with crossbar [20]. A grid 49-loudspeaker array and a sparse 21-loudspeaker array [20] were compared. We assumed that, by measuring the performance in all directions, any reflection is irrelevant. Therefore, no walls were modeled. The cross-section ($x = 0$) top-view of the environment is depicted in Figure 1, with coordinates (x, y, z) pointing into the paper, upwards and to the right. The red dot is a reference microphone, the blue dots are loudspeakers and the green dots represent evaluation microphones. In 3D, the aperture was a L_x = 0.5 m by L_y = 0.5 m window, with a crossbar of width W_+ = 0.065 m. Hence, the aperture consisted of four squares ($\hat{P} = 4$) with $\Delta L_x = (L_x - W_+)/2 = \Delta L_y$. The 2D model was a L_y-wide aperture with a crossbar of width W_+ and $\hat{P} = 2$.

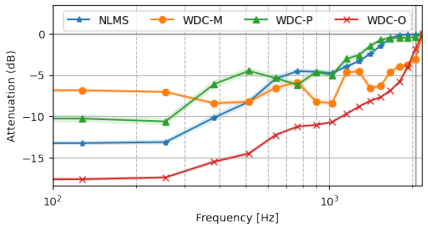

Fig. 4: $\overline{\text{SEG}_f}(k)$, with very narrow 99% confidence interval for grid array simulations in 3D, canceling rumbler-siren noise.

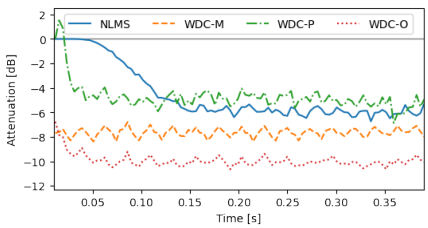

Fig. 5: First 0.4 s of SEG_t 3D grid array results for all controllers, showing long the convergence time of NLMS controller.

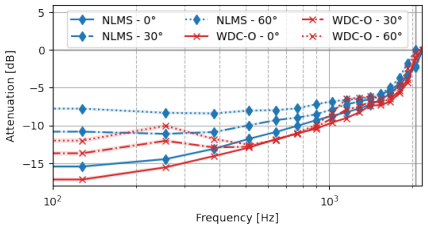

Fig. 6: $\overline{\text{SEG}_f}(k)$ for NLMS and WDC-O, with very narrow 99% confidence interval. 3D results for white noise signal, at 0°, 30°and 60°angle.

All controllers used one reference microphone in the aperture origin and were implemented with the sparse and grid array. The NLMS was tested with 32 (2D) and 128 (3D) error microphones in the control region. The optimal wave-domain controller (WDC-O) used a window-size of 125 ms. Additionally, algorithmic delay compensation was modeled by two approaches. The first uses a reference microphone positioned 1.4 m outside the aperture, implemented with a window-size of 3.9 ms (WDC-M), The second is a wave-domain controller with an auto regressive predictor (WDC-P). The wave-domain algorithms used a 75% STFT overlap.

Sample rate was set at $f_s = 2^{14}$ Hz. A fixed air temperature and density (ρ_0) were used, setting constant speed of sound at $c = 343$ m/s. To measure the performance of the controllers over time with a changing frequency spectrum, a rumbler-siren signal (Figure 2a) of 4 s was used as noise. Additionally, white noise and airplane noise (Figure 2b) were tested. Following existing studies [12], we evaluate the performance up to 2 kHz and for three incident angles: 0°, 30°and 60°. The performance was evaluated on the boundary of control regions $\mathbb{D}_{2D}$ and $\mathbb{D}_{3D}$ at 30 and 128 evenly distributed evaluation microphones, respectively. We define the segmental SNR in dB, summed over all evaluation microphones e as:

$$\text{SEG}_f(k,m) = 10\log_{10}\frac{\sum_e^E |d_e(k,m)|^2}{\sum_e^E |d_e(k,m)+y_e(k,m)|^2} \qquad (14)$$

where d_e is the noise signal and y_e is the loudspeaker array signal. We average $\text{SEG}_f(k,m)$ over frequency and time, to get insights per frequency bin ($\overline{\text{SEG}_f}(k)$), per hop ($\text{SEG}_t(m)$) and in total (SNR). Performance was calculated over signal blocks with an 8 ms STFT with 50% overlap.

4.3. Attenuation performance

Table 1 shows the performance for all signals at 0°incident angle, where the grid outperformed the sparse array. WDC-O generated more attenuation than NLMS, when cancelling rumbler-siren noise, especially at higher frequencies as shown in Figure 4. Additionally,

Noise type	**Rumbler siren**		**Airplane Noise**		**White Noise**	
Array	G	S	G	S	G	S
NLMS	-5.2	-3.5	-7.6	-4.5	-9.2	-4.3
WDC-M	-6.1	-1.3	-6.6	-2.0	-8.1	-2.8
WDC-P	-4.0	-2.2	-	-	-	-
WDC-O	-10.6	-4.9	-10.6	-4.7	-10.0	-4.1

Table 1: 3D, 0°angle, SNR for all controllers, with grid (G) and sparse (S) arrays. Attenuation is given in decibel (dB).

Figure 5 shows the slow convergence of NLMS, fast convergence of WDC-P, and instant convergence of WDC-O and WDC-M. Following Figure 6, WDC-O outperformed NLMS with better attenuation for each incident angle. When comparing algorithmic delay compensation methods, WDC-M slightly outperformed the WDC-P, with a grid array setup. Moreover, for WDC-P, a trade-off between prediction accuracy and algorithm performance was apparent so an optimal window-size is found, shown in Figure 3. However this optimum highly depends on the type of signal. For signals that are better predictable, the optimal window-size is larger. Finally, all controllers perform better at lower frequencies, except for WDC-M. For its short window-size, relatively large phase-shifts in the blockwise signal processing result in the loss of parts of the signal.

The grid array outperformed the sparse array, confirming prior studies [31]. Besides, both the performance of white noise cancelling, and occurrence of long convergence time of the NLMS controller is in line with existing literature [12,32]. For a stationary noise source, slow convergence is no issue as NLMS weights could be calculated offline. However, we expect that slow convergence limits the performance of an online NLMS in case of a moving noise source. In contrast, the wave-domain controller is expected to perform better. Further investigation into performance for moving sources is necessary. Additionally, the trade-off apparent for WDC-P (Figure 3) follows prior results [15]. Improving algorithmic delay compensation methods, with a combination of microphone placement and prediction, or employing machine-learning, is a worthwhile continuation of this work. Offline calculation of filter-weights in WDC-O is a major advantage over closed-loop algorithms. Finally, we suggest to investigate STFT wrapping in wave-domain control algorithms, to improve performance at shorter window-sizes.

5. CONCLUSION

We proposed a new approach to ANC for apertures based on wave-domain processing with algorithmic delay compensation. We compared the new algorithm with a multiple-error Normalized LMS system for both sparse and grid arrays. Our 3D results showed that an ideal wave-domain algorithm obtains an average global attenuation of - 10.6 dB up to 2 kHz for a 0.5 m window, compared to - 5.2 dB for the LMS based algorithm when a grid array is used for attenuation rumbler-siren noise. Algorithmic delay compensation by microphone placement is preferred over predictor methods. Improving on delay solutions is a logical continuation of our work. Our results show that the use of wave-domain ANC algorithms for open windows is natural for addressing the noise pollution problems of modern society as the new method requires neither time to converge nor error microphones, and operates at a low computational effort due to off-line weight calculation.

6. REFERENCES

[1] W. H. Organization, *Burden of disease from environmental noise: Quantification of healthy life years lost in Europe*, 2011.

[2] L. Bhan and G. Woon-Seng, "Active acoustic windows: Towards a quieter home," *IEEE Potentials*, vol. 35, no. 1, pp. 11–18, 2016.

[3] S. M. Kuo, S. Mitra, and W.-S. Gan, "Active noise control system for headphone applications," *IEEE Transactions on Control Systems Technology*, vol. 14, no. 2, pp. 331–335, 2006.

[4] S. J. Elliott, "Down with noise (active noise control)," *IEEE spectrum*, vol. 36, no. 6, pp. 54–61, 1999.

[5] S. Wang, J. Yu, X. Qiu, M. Pawelczyk, A. Shaid, and L. Wang, "Active sound radiation control with secondary sources at the edge of the opening," *Applied Acoustics*, vol. 117, pp. 173–179, 2017.

[6] B. Lam, S. Elliott, J. Cheer, and W.-S. Gan, "Physical limits on the performance of active noise control through open windows," *Applied Acoustics*, vol. 137, pp. 9–17, 2018.

[7] S. M. Kuo and D. R. Morgan, "Active noise control: a tutorial review," *Proceedings of the IEEE*, vol. 87, no. 6, pp. 943–973, 1999.

[8] L. Bhan, T. Murao, C. Shi, W.-S. Gan, and S. Elliott, "Feasibility of the full-rank fixed-filter approach in the active control of noise through open windows," in *INTER-NOISE and NOISE-CON Congress and Conference Proceedings*, vol. 253, no. 5. Institute of Noise Control Engineering, 2016, pp. 3548–3555.

[9] C. Shi, T. Murao, D. Shi, B. Lam, and W.-S. Gan, "Open loop active control of noise through open windows," in *Proceedings of Meetings on Acoustics 172ASA*, vol. 29, no. 1. Acoustical Society of America, 2016, p. 030007.

[10] C. Shi, N. Jiang, H. Li, D. Shi, and W.-S. Gan, "On algorithms and implementations of a 4-channel active noise canceling window," in *2017 International Symposium on Intelligent Signal Processing and Communication Systems (ISPACS)*. IEEE, 2017, pp. 217–221.

[11] B. Kwon and Y. Park, "Interior noise control with an active window system," *Applied Acoustics*, vol. 74, no. 5, pp. 647–652, 2013.

[12] T. Murao and M. Nishimura, "Basic study on active acoustic shielding," *Journal of Environment and Engineering*, vol. 7, no. 1, pp. 76–91, 2012.

[13] Y. J. Wu and T. D. Abhayapala, "Theory and design of soundfield reproduction using continuous loudspeaker concept," *IEEE Transactions on Audio, Speech, and Language Processing*, vol. 17, no. 1, pp. 107–116, 2008.

[14] W. Jin and W. B. Kleijn, "Theory and design of multizone soundfield reproduction using sparse methods," *IEEE/ACM Transactions on Audio, Speech, and Language Processing*, vol. 23, no. 12, pp. 2343–2355, 2015.

[15] J. Donley, C. Ritz, and W. B. Kleijn, "Active speech control using wave-domain processing with a linear wall of dipole secondary sources," in *2017 IEEE International Conference on Acoustics, Speech and Signal Processing (ICASSP)*. IEEE, 2017, pp. 456–460.

[16] J. Zhang, T. D. Abhayapala, W. Zhang, P. N. Samarasinghe, and S. Jiang, "Active noise control over space: A wave domain approach," *IEEE/ACM Transactions on audio, speech, and language processing*, vol. 26, no. 4, pp. 774–786, 2018.

[17] J. Donley, C. Ritz, and W. B. Kleijn, "On the comparison of two room compensation/dereverberation methods employing active acoustic boundary absorption," in *2018 IEEE International Conference on Acoustics, Speech and Signal Processing (ICASSP)*. IEEE, 2018, pp. 221–225.

[18] S. Spors, H. Wierstorf, A. Raake, F. Melchior, M. Frank, and F. Zotter, "Spatial sound with loudspeakers and its perception: A review of the current state," *Proceedings of the IEEE*, vol. 101, no. 9, pp. 1920–1938, 2013.

[19] L. P. Miller, "An analysis of acoustic beam-forming with sparse transducer arrays for active control," 2018, mSc. Thesis, The Pennsylvania State University, The Graduate School, College of Engineering.

[20] K. Downey, "Loudspeaker array and testing facilities for performing large volume active noise cancelling measurements," 2020, mSc. Thesis, The Pennsylvania State University, The Graduate School, College of Engineering.

[21] E. G. Williams, *Fourier acoustics: sound radiation and nearfield acoustical holography*. Elsevier, 1999.

[22] F. J. Fahy, *Foundations of engineering acoustics*. Elsevier, 2000.

[23] A. D. Pierce, *Acoustics: an introduction to its physical principles and applications*. Springer, 2019.

[24] J. Fliege and U. Maier, "The distribution of points on the sphere and corresponding cubature formulae," *IMA Journal of Numerical Analysis*, vol. 19, no. 2, pp. 317–334, 1999.

[25] G. H. Golub and C. F. van Loan, *Matrix Computation*. Blatimore, MD, USA: Johns Hopkins Univ. Press, 1996.

[26] R. A. Kennedy, P. Sadeghi, T. D. Abhayapala, and H. M. Jones, "Intrinsic limits of dimensionality and richness in random multipath fields," *IEEE Transactions on Signal processing*, vol. 55, no. 6, pp. 2542–2556, 2007.

[27] M. Vetterli, J. Kovačević, and V. K. Goyal, *Foundations of signal processing*. Cambridge University Press, 2014.

[28] R. H. Shumway, D. S. Stoffer, and D. S. Stoffer, *Time series analysis and its applications*. Springer, 2000, vol. 3.

[29] S. J. Elliott and P. A. Nelson, "Active noise control," *IEEE signal processing magazine*, vol. 10, no. 4, pp. 12–35, 1993.

[30] C. H. Hansen, S. D. Snyder, X. Qiu, L. A. Brooks, and D. J. Moreau, *Active control of noise and vibration*. Spon London, 1997.

[31] B. Lam, C. Shi, D. Shi, and W.-S. Gan, "Active control of sound through full-sized open windows," *Building and Environment*, vol. 141, pp. 16–27, 2018.

[32] S. Elliott, I. Stothers, and P. Nelson, "A multiple error lms algorithm and its application to the active control of sound and vibration," *IEEE Transactions on Acoustics, Speech, and Signal Processing*, vol. 35, no. 10, pp. 1423–1434, 1987.